

Two-dimensional point singularity model of a low-Reynolds-number swimmer near a wall

Darren G. Crowdy

Department of Applied Mathematics, Imperial College, London, United Kingdom

Yizhar Or

Faculty of Mechanical Engineering, Technion-Israel Institute of Technology, Haifa, Israel

(Received 2 November 2009; revised manuscript received 28 January 2010; published 11 March 2010)

This paper studies a simple two-dimensional model of a swimmer at low-Reynolds-number near a no-slip wall by utilizing methods of complex analysis. The swimmer is propelled by purely tangential surface deformations and is modeled by moving point singularities. The nonlinear dynamics of the swimmer is formulated explicitly, and its motion near the wall is fully characterized. The results show qualitative agreement with predictions of three-dimensional models and with motion experiments on a robotic swimmer. The success and simplicity of the model suggest that it will provide a simple way to study the dynamics of low-Reynolds-number swimmers in more complicated geometries.

DOI: [10.1103/PhysRevE.81.036313](https://doi.org/10.1103/PhysRevE.81.036313)

PACS number(s): 47.63.mf, 02.30.Fn, 47.10.Fg, 47.63.Gd

I. INTRODUCTION

The locomotion of micro-organisms [1,2] and of tiny robotic swimmers [3,4] is governed by low-Reynolds-number hydrodynamics, where viscous effects dominate and inertial effects are negligible [5–7]. A vast majority of the literature on the theory of low-Reynolds-number locomotion studies the case of unbounded fluid domain [8–10]. However, in reality, micro-organisms often swim in confined environments and interact hydrodynamically with the boundary. While the effects of a boundary on inert rigid bodies in viscous fluid were widely studied [11,12], the behavior of microswimmers near a boundary was studied analytically only for specific scenarios [13]. Nevertheless, experimental observations indicate that the presence of a boundary significantly affects the dynamic behavior and motion trajectories of swimming micro-organisms. Examples are *E. coli* swimming in circles above a flat surface [14], accumulation of bacteria and sperm cells near boundaries [15,16], shear-induced periodic orbits of bacteria and larvae [17,18], and interesting “dancing” motion of pairs of *Volvox* algae [19]. Some of these phenomena were verified using numerical simulation [20–22], but only few physical explanations have been proposed. The work of Berke *et al.* [16] studies the hydrodynamic attraction of swimming micro-organisms to surfaces by modeling the swimmer as a force dipole singularity. This simple model captures the attraction of the swimmer but predicts crashing into the surface in finite time in contrast to the

experimental findings. Moreover, the analysis in [16] did not study the *dynamics* of swimming near a boundary and the resulting trajectories. The work of Zargar *et al.* [23] studies the influence of a wall on the theoretical model of the three-linked-spheres swimmer [9]. The average dynamics in the limit of small strokes is formulated for the cases of very large and very small distances from the wall. It is shown that the swimmer can move parallel to the wall, and some arguments are made regarding the dynamic stability of these solutions. In the work [24], the dynamics of low-Reynolds-number swimming near a plane wall is studied for simple theoretical models of swimmers propelled by rotating spheres. In particular, the motion of a swimmer consisting of two rotating spheres connected by a thin rod [Fig. 1(a)] was analyzed. It was found that when the spheres are rotated in unequal velocities, the swimmer has a solution of steady translation parallel to the wall. This solution is *marginally stable*, and under small perturbation, the swimmer exhibits oscillatory motion along the wall, as shown in Fig. 1(b). The results were recently verified experimentally on a macroscale robotic prototype swimming in a highly viscous fluid [25]. Propulsion was generated by rotating two cylinders via DC motors which were mounted on a floatation system in order to balance the gravitational load and keep the motion in a horizontal plane [Fig. 1(d)]. Motion of the swimmer was measured and recorded, showing remarkable qualitative agreement with the theoretical predictions [Fig. 1(c)].

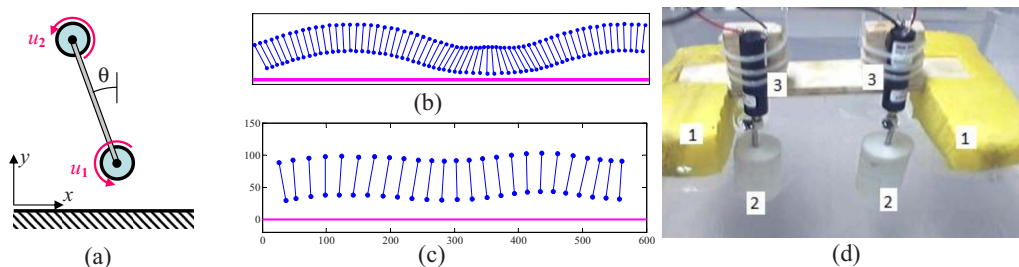


FIG. 1. (Color online) (a) The two-sphere swimmer model from [24]. (b) Simulation of the two-sphere swimmer near a wall. (c) Experimental measurements of motion of the swimmer from [25] near a wall. (d) The robotic two-cylinder swimmer prototype from [25].

In this paper we study the dynamics of a simple swimmer model near an infinite no-slip wall in two dimensions by utilizing methods of complex analysis. Such techniques were used previously for analyzing planar axisymmetric swimmer models in unbounded fluid domains [8,26,27]. The justification for using a two-dimensional model lies in the fact that in many of existing theoretical models of low-Reynolds-number locomotion in three dimensions, the swimmer possesses symmetry about its sagittal (median) plane, e.g., [24,28], or even about its longitudinal axis, e.g., [9,10,27], so that its motion is confined to a plane even though the flow around it is fully three-dimensional. Therefore, it is expected that a two-dimensional model will correctly capture the essential ingredients and qualitative dynamic behavior of such swimmers. We focus here on a particular propulsion mechanism called *treadmilling*, in which the boundary of the swimmer undergoes purely tangential surface deformations while the shape of the swimmer remains fixed. Similar models were used in the literature as a simplification to the synchronized action of short cilia on the surface of motile cells such as *Opalina* and *Volvox* [29–31]. The advantage of this simplification is that it avoids the complications associated with the changing shape of the swimmer while focusing solely on its hydrodynamic interaction with the boundary.

II. COMPLEX VARIABLE FORMULATION

We begin by reviewing the complex variable formulation of Stokes flow in two dimensions. Stokes equations that describe the motion of an incompressible viscous fluid are given by $-\nabla p + \eta \nabla^2 \mathbf{v} = 0$, $\nabla \cdot \mathbf{v} = 0$, where \mathbf{v} is the fluid velocity field, p is the pressure distribution, and η is the fluid viscosity. In two dimensions, these equations can be reformulated by introducing the notion of a *stream function* $\psi(x, y)$, such that the x, y components of the fluid velocity are given by $v_x = \partial \psi / \partial y$, $v_y = -\partial \psi / \partial x$, and Stokes equations then reduce to the biharmonic equation $\nabla^4 \psi = 0$. Using complex coordinates $z = x + iy$, it can be shown [32,33] that the general solution for ψ is given by

$$\psi = \text{Im}[\bar{z}f(z) + g(z)], \tag{1}$$

where $f(z)$ and $g(z)$, called *Goursat functions*, are analytic functions that are allowed to have isolated singularities in order to model various flows of interest. The velocity field is then given in terms of $f(z)$ and $g(z)$ as

$$v_x + iv_y = -2i \frac{\partial \psi}{\partial \bar{z}} = -f(z) + \overline{zf'(z)} + \overline{g'(z)}, \tag{2}$$

where $f'(z) = df/dz$. The fluid pressure p and vorticity ω are related to $f(z)$ via [32]

$$p = 4\mu \text{Re}[f'(z)], \quad \omega = -4 \text{Im}[f'(z)]. \tag{3}$$

To solve a Stokes flow problem in two dimensions, it is enough to determine the two analytic functions $f(z)$ and $g(z)$. This is usually done by making use of the boundary conditions.

The usual singular solutions of Stokes flow [33,34] (Stokeslets, stresslets, rotlets, etc.) manifest themselves

within this complex variable formulation as singularities of the two functions $f(z)$ and $g(z)$. For example, consider a concentrated force whose magnitude and angle are represented by the complex number μ , which is applied at a given point z_0 . The resulting flow, which is called a *Stokeslet* at z_0 [33], is associated with a solution where $f(z)$ and $g'(z)$ are given by

$$f(z) = \mu \ln(z - z_0), \quad g'(z) = -\bar{\mu} \ln(z - z_0) - \frac{\mu \bar{z}_0}{z - z_0}. \tag{4}$$

Using Eq. (2), the resulting velocity field is given by

$$v_x + iv_y = -\mu \ln|z - z_0|^2 + \frac{\bar{\mu}(z - z_0)^2}{|z - z_0|^2}.$$

Note that the singularities in $g'(z)$ were chosen according to those in $f(z)$ in order to ensure that the velocity field is both single-valued and logarithmically singular at z_0 [i.e., the non-logarithmic term in $g'(z)$ must be added to ensure that the velocity does not blow up like $1/|z - z_0|$]. For example, the (x, y) components of the velocity field due to a unit force applied at (x_0, y_0) in the x direction are given by

$$v_x(x, y) = -2 \ln r + \frac{2(x - x_0)^2}{r^2},$$

$$v_y(x, y) = \frac{2(x - x_0)(y - y_0)}{r^2},$$

where $r = \sqrt{(x - x_0)^2 + (y - y_0)^2}$. In the far field $r \rightarrow \infty$, the velocity field becomes unbounded and this feature is at the heart of the familiar Stokes paradox [35]. Next, the choice of $f(z), g'(z)$ as

$$f(z) = \frac{\mu}{z - z_0}, \quad g'(z) = \frac{\mu \bar{z}_0}{(z - z_0)^2}$$

is called a *stresslet* at z_0 . In this case, $g'(z)$ was imposed by the choice of $f(z)$ in order to ensure that the velocity field is singular like $1/|z - z_0|$ (rather than $1/|z - z_0|^2$). Physically, this case corresponds to the flow due to a limiting case of a pair of point forces drawing infinitesimally close together, with equal and opposite strengths tending to infinity at a rate inversely proportional to their separation.

Note, however, that $g(z)$ can additionally have its own singularities, independently of those imposed by the choice of $f(z)$. For example, $g(z) = c \ln(z - z_0)$, where $c \in \mathbb{R}$ is called a source (or sink) at z_0 while if $c \in i\mathbb{R}$ then it is called a rotlet, which corresponds to a *rotational torque* applied at the point z_0 . A simple pole of $g(z)$ is an irrotational dipole singularity, a double pole of $g(z)$ is an irrotational quadrupole, and so on. Any swimmer in a Stokes flow will locally generate a flow that can equivalently be modeled by some distribution of Stokes flow singularities (positioned inside or on the boundary of its body). This equivalent singularity distribution is generally a complicated function of the swimmer’s size and shape, its chosen swimming protocol, and its local effect on the fluid around it. In many cases, a complicated swimmer is *approximated* by an equivalent singularity de-

scription, which consists of a small number of moving point singularities [16,19,30], as we shall do here.

In the presence of a no-slip wall, the solution associated with each point singularity must be modified so that the velocity field satisfies the no-slip boundary condition on the wall. We now show how this is done in the complex formulation of two-dimensional Stokes flow in analogy to the classical method of “image system” in three dimensions [34]. In the case where the wall is located at $\text{Re}(z)=0$, the key idea is that a point singularity at z_0 must be augmented by singularities at the image point \bar{z}_0 . Then, using the expression for the fluid velocity in Eq. (2) and requiring that it vanishes on the wall $\bar{z}=z$, one obtains $-f(z)+zf'(z)+g'(z)=0$. This implies that

$$g'(z) = \bar{f}(z) - zf'(z), \quad (5)$$

which is a functional equation determining $g'(z)$ from $f(z)$ and its conjugate function $\bar{f}(z)$, defined as $\bar{f}(z)=\overline{f(\bar{z})}$. For example, we now show how to find the image singularity of a Stokeslet of strength μ at position z_0 above a no-slip wall. Let

$$f(z) = \mu \ln(z - z_0) + \lambda \ln(z - \bar{z}_0) + \frac{\epsilon}{z - z_0}, \quad (6)$$

where λ and ϵ are constants to be determined. This gives the required Stokeslet at z_0 with both a Stokeslet and a stresslet at the image point \bar{z}_0 . Substitution of Eq. (6) into relation (5) implied by the no-slip condition on the wall gives

$$g'(z) = \bar{\mu} \ln(z - \bar{z}_0) + \bar{\lambda} \ln(z - z_0) + \frac{\bar{\epsilon}}{z - \bar{z}_0} - \frac{\mu z}{z - z_0} - \frac{\lambda z}{z - \bar{z}_0} + \frac{\epsilon z}{(z - \bar{z}_0)^2}.$$

We know from above that near z_0 , the function $g'(z)$ must have the local behavior given by Eq. (4). Hence we must pick $\lambda = -\mu$, $\epsilon = \bar{\mu}(\bar{z}_0 - z_0)$ in order to obtain

$$g'(z) = -\bar{\mu} \ln(z - \bar{z}_0) - \frac{\mu z_0}{z - z_0} + \bar{\mu} \ln(z - \bar{z}_0) + \frac{\mu \bar{z}_0}{z - \bar{z}_0} + \frac{\epsilon z_0}{(z - \bar{z}_0)^2} + \frac{\epsilon(\bar{z}_0 - z_0)}{(z - \bar{z}_0)^2} - \frac{(\mu + \bar{\mu})(z_0 - \bar{z}_0)}{z - \bar{z}_0}.$$

The first two terms on the right-hand side are associated with the Stokeslet at z_0 , the third and fourth terms are associated with the Stokeslet at \bar{z}_0 , the fifth term is associated with the stresslet at \bar{z}_0 , the penultimate term gives a source dipole, while the final term is a removable singularity. We conclude that the image system for a Stokeslet near a wall is a Stokeslet of the opposite sign together with a stresslet (force dipole) and a source dipole. Qualitatively, this is the same image distribution originally identified by Blake [36] (using Fourier transforms) for a three-dimensional Stokeslet near a wall.

III. TREADMILLING SWIMMER MODEL

We now describe our treading swimmer model, whose body is a circle of radius ϵ with a moving center

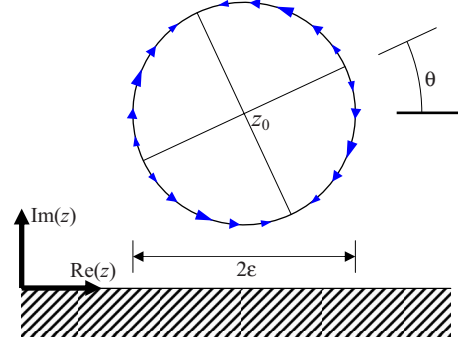


FIG. 2. (Color online) The treading circular swimmer.

$z_0(t)=x(t)+iy(t)$. We endow the swimmer with a distinguished direction making an angle $\theta(t)$ with the real axis, which can be interpreted as the direction of its head. It is with respect to this direction that we suppose that cilia (or some other surface actuators) induce a tangential velocity profile given by $U(\phi, t)=2V \sin[2(\phi - \theta)]$, where ϕ is the angle measured from the positive x direction and $\phi = \theta$ is the direction of the head of the swimmer (see Fig. 2). V is a constant whose magnitude sets the time scale for the treading action. The velocity profile $U(\phi, t)$ can be rewritten as

$$U(\phi, t) = c(t)e^{2i\phi} + \bar{c}(t)e^{-2i\phi}, \quad \text{where } c(t) = -iVe^{-2i\theta(t)}. \quad (7)$$

Note that in unbounded fluid, this velocity profile does *not* result in any self-propulsion of the organism due to its symmetry about two axes. We focus here on such a non-self-propelling swimmer in order to isolate and understand just the hydrodynamic interaction of the swimmer and the wall.

We now derive the solution for the flow around this swimmer in *unbounded fluid* and show that it consists of a stresslet and a quadrupole at z_0 . Suppose that the center of the swimmer $z_0(t)=x(t)+iy(t)$ moves in a translational velocity $\dot{x}(t)+i\dot{y}(t)$ and that the swimmer rotates with an angular velocity $\Omega(t)$. The velocity field around the swimmer satisfies the boundary condition

$$v_x + iv_y = -\tilde{f}(z) + z\tilde{f}'(z) + \bar{g}'(z) = \dot{x} + i\dot{y} + [\epsilon\Omega + U(\phi, \theta)] \frac{dz}{ds} \quad (8)$$

on $|z - z_0| = \epsilon$, where dz/ds is the complex unit tangent to the boundary and $\tilde{f}(z)$ and $\bar{g}'(z)$ must be found. For convenience, the time dependency in Eq. (8) was suppressed. We seek solutions for $\tilde{f}(z)$ and $\bar{g}'(z)$ having the form

$$\tilde{f}(z) = \frac{\mu}{z - z_0} + \tilde{f}_0 + \tilde{f}_1(z - z_0),$$

$$\bar{g}'(z) = \frac{\beta}{(z - z_0)^3} + \frac{\alpha}{(z - z_0)^2} + \bar{g}_0. \quad (9)$$

In Eq. (9), we have allowed for a uniform velocity and solid body rotation in the far field which we expect to be deter-

mined by the ambient flow. Owing to the fact that the swimmer exerts no net force or torque on the fluid, we have omitted any Stokeslet or rotlet singularities.

We now use the boundary condition (8) to find relations between the coefficients in Eq. (9) and the velocity of the swimmer. We make use of the fact that on the boundary $|z - z_0| = \epsilon$, the following relations hold:

$$z - z_0 = \frac{\epsilon^2}{z - z_0}, \quad \frac{dz}{ds} = \frac{i(z - z_0)}{\epsilon}.$$

Substituting into Eq. (8) and equating coefficients of different powers of $(z - z_0)$, one obtains

$$\dot{x} + i\dot{y} = -\tilde{f}_0 + \tilde{f}_1 z_0 + \tilde{g}_0, \quad i\Omega = -(\tilde{f}_1 - \tilde{f}_1),$$

$$\mu = -i\bar{c}\epsilon, \quad \alpha = \mu\bar{z}_0, \quad \beta = \mu\epsilon^2 - i\bar{c}\epsilon^3 = 2\mu\epsilon^2. \quad (10)$$

Thus, the swimmer has an equivalent ‘‘point singularity’’ description with a stresslet of strength μ and a quadrupole of strength $2\epsilon^2\mu$ at z_0 . We now set the time scale of the motion by letting $V = \epsilon^{-1}$, so that $\mu(t) = e^{2i\theta(t)}$. Interestingly, note that the orientation angle of the resulting stresslet is twice the angle of the swimmer’s orientation. This differs from the analysis in [16], in which the stresslet (force dipole) is assumed to have the same orientation as the swimmer. The physical explanation to this difference is as follows. The tangential velocity profile given in Eq. (7) has twofold periodicity along the circular boundary of the swimmer. Therefore, it has two axes of symmetry, unlike the treadmiller model in [37] and the twirling torus in [27], which have only one axis of symmetry. (This is also the reason why our treadmill swimmer does not move at all in unbounded fluid, whereas the swimmers in [9,27] move along the axis of symmetry.)

The solution in Eq. (9) can be viewed as an ‘‘inner solution’’ describing the flow generated in the vicinity of the swimmer without accounting for the effect of the wall. We now model the swimmer as two point singularities as given in Eq. (9) above an infinite no-slip wall at the real axis in order to obtain an ‘‘outer solution’’ for the flow far from the swimmer. The motion of the swimmer will then be determined by matching the inner and outer solutions. Consider a swimmer represented by stresslet and quadrupole singularities at z_0 , which is placed above a no-slip wall at $\text{Re}(z) = 0$. Let

$$f(z) = \frac{\mu}{z - z_0} + \frac{\delta}{z - \bar{z}_0} + \frac{\lambda}{(z - \bar{z}_0)^2} + \frac{\chi}{(z - \bar{z}_0)^3}, \quad (11)$$

where δ , λ , and χ are parameters to be determined. Utilizing the functional relation (5) implied by the no-slip condition on the wall, $g'(z)$ is obtained as

$$g'(z) = \frac{(\bar{\delta} + \mu)}{z - z_0} + \frac{(\bar{\lambda} + z_0\mu)}{(z - z_0)^2} + \frac{\bar{\chi}}{(z - z_0)^3} + \left[\frac{\bar{\mu} + \delta}{z - \bar{z}_0} + \frac{\bar{\delta}\bar{z}_0 + 2\lambda}{(z - \bar{z}_0)^2} + \frac{2\lambda\bar{z}_0 + 3\chi}{(z - \bar{z}_0)^3} + \frac{3\chi\bar{z}_0}{(z - \bar{z}_0)^4} \right]. \quad (12)$$

The terms in square brackets are grouped together because

they are image singularities at \bar{z}_0 (the reflected point in the wall). Matching the strength of the singularities at z_0 in Eqs. (11) and (12) with those in Eq. (9) gives

$$\delta = -\bar{\mu}, \quad \bar{\lambda} + z_0\mu = \alpha = \mu\bar{z}_0, \quad \bar{\chi} = \beta = 2\mu\epsilon^2. \quad (13)$$

Next, in order to match the regular part of the outer and inner solutions, we define the constants f_0 , f_1 , and g_0 as the first few coefficients of the Taylor expansion of the regular parts of $f(z)$ and $g'(z)$ in Eqs. (11) and (12) at the singularity position z_0 , so that

$$f(z) = \frac{\mu}{z - z_0} + f_0 + f_1(z - z_0) + \dots, \\ g'(z) = \frac{(\bar{\lambda} + z_0\mu)}{(z - z_0)^2} + \frac{\bar{\chi}}{(z - z_0)^3} + g_0 + \dots. \quad (14)$$

Using Eqs. (11)–(13), we deduce the explicit formulas

$$f_0 = \frac{\delta}{z_0 - \bar{z}_0} + \frac{\lambda}{(z_0 - \bar{z}_0)^2} + \frac{\chi}{(z_0 - \bar{z}_0)^3}, \\ f_1 = -\frac{\delta}{(z_0 - \bar{z}_0)^2} - \frac{2\lambda}{(z_0 - \bar{z}_0)^3} - \frac{3\chi}{(z_0 - \bar{z}_0)^4}, \\ g_0 = \frac{2\lambda + \bar{\delta}\bar{z}_0}{(z_0 - \bar{z}_0)^2} + \frac{(2\lambda\bar{z}_0 + 3\chi)}{(z_0 - \bar{z}_0)^3} + \frac{3\chi\bar{z}_0}{(z_0 - \bar{z}_0)^4}. \quad (15)$$

We now equate f_0 , f_1 , and g_0 in Eq. (14) with \tilde{f}_0 , \tilde{f}_1 , and \tilde{g}_0 in Eq. (9). Using relations (13) and (15), the linear and angular velocities of the swimmer are finally obtained as

$$\dot{x} + i\dot{y} = -\frac{2\mu}{(z_0 - \bar{z}_0)} - \frac{2\epsilon^2(\bar{\mu} + 3\mu)}{(z_0 - \bar{z}_0)^3}, \\ \Omega = -i \left[\frac{(\bar{\mu} - \mu)}{(z_0 - \bar{z}_0)^2} + \frac{6\epsilon^2(\bar{\mu} - \mu)}{(z_0 - \bar{z}_0)^4} \right]. \quad (16)$$

Since $\Omega = d\theta/dt$, substitution of $\mu = \exp[2i\theta(t)]$ into Eq. (16) yields a system of three nonlinear ordinary differential equations in $x(t)$, $y(t)$, $\theta(t)$, which is written explicitly as

$$\dot{x} = -\frac{\sin(2\theta)}{y} \left(1 - \frac{\epsilon^2}{2y^2} \right), \quad \dot{y} = \frac{\cos(2\theta)}{y} \left(1 - \frac{\epsilon^2}{y^2} \right), \\ \dot{\theta} = \frac{\sin(2\theta)}{2y^2} \left(1 - \frac{3\epsilon^2}{2y^2} \right). \quad (17)$$

Note that Eq. (17) is independent of the horizontal position x of the swimmer as expected.

IV. DYNAMIC ANALYSIS

We now analyze the dynamic behavior of the swimmer model. We begin with the limit case of a point swimmer $\epsilon = 0$ and compare with the analysis of the three-dimensional case in [16]. When $\epsilon = 0$ the swimmer is represented by a point stresslet with no superposed quadrupole contribution.

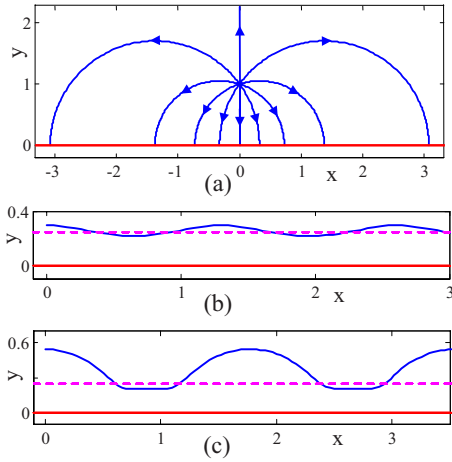


FIG. 3. (Color online) Swimmer trajectories in xy plane. (a) A point swimmer with $y(0)=1$ and different values of $\theta(0)$. (b) A swimmer with $\epsilon=0.2$ for $\theta(0)=-\pi/4$, $y(0)=y_e+0.05$. (c) A swimmer with $\epsilon=0.2$ for $\theta(0)=-\pi/4$, $y(0)=y_e+0.3$. The dashed lines are $y=y_e$.

From the dynamic equation [Eq. (17)], it is seen that for the orientations $\theta=\{0, \pm\pi/2, \pi\}$, the motion of the swimmer is a pure translation in the vertical (y) direction, so that at $\theta=0, \pi$ the swimmer moves away from the wall and at $\theta=\pm\pi/2$ the swimmer moves toward the wall and crashes into it in finite time. Moreover, from the equation for the angular velocity $\dot{\theta}$ in Eq. (17), it can be seen that the swimmer reorients itself toward $\theta=\pm\pi/2$. As a result, for any initial position and orientation, the swimmer will eventually reach the wall in finite time, except for the cases $\theta=0, \pi$, for which the swimmer moves away from the wall (with any small perturbation leading to reorientation and returning back to the wall). Examples of motion trajectories of the point swimmer under different initial orientations are shown in Fig. 3(a). These observations are consistent with the analysis of Berke *et al.* [16]. Moreover, the expressions for \dot{y} and $\dot{\theta}$ in Eq. (17) for the case $\epsilon=0$ are similar to those derived in [16], although the powers of y in the denominator are different. Finally, Eq. (17) indicates that when the distance from the wall y is large, the reorientation rate $\dot{\theta}$ is slower than the vertical velocity \dot{y} , which again agrees with the observation and derivation of the different time scales in [16].

Next, we analyze the case of a finite-size swimmer $\epsilon \neq 0$. In this case, at orientations $\theta_0=\{0, \pm\pi/2, \pi\}$, the motion of the swimmer is again a purely vertical translation. In these cases, the differential equation governing the evolution of the vertical coordinate $y(t)$ can be solved in closed form, and the solution under initial condition $y(0)=y_0$ is given implicitly as $y^2 + \epsilon^2 \ln(y^2 - \epsilon^2) = y_0^2 + \epsilon^2 \ln(y_0^2 - \epsilon^2) + 2st$, where $s = \cos(2\theta_0) = \pm 1$. This solution shows that for $\theta_0=0, \pi$ the swimmer moves away from the wall. For $\theta_0=\pm\pi/2$, the swimmer approaches the wall only asymptotically (i.e., $y \rightarrow \epsilon^+$ as $t \rightarrow \infty$) instead of crashing into it. This behavior agrees with physical arguments stating that finite-time establishment of contact between solid bodies in Stokes flow is impossible due to development of infinitely large *lubrication forces* [35].

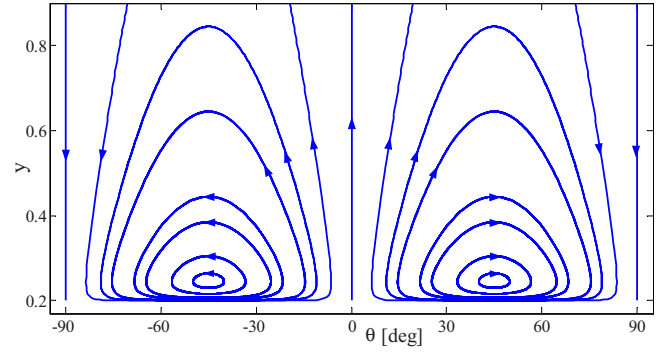


FIG. 4. (Color online) Phase portrait of trajectories in (θ, y) plane for the treadmilling swimmer with $\epsilon=0.2$.

Another type of solution of Eq. (17) which is impossible for a point swimmer is pure translation *parallel to the wall*. This motion is obtained for a specific distance from the wall given by $y_e = \sqrt{3/2}\epsilon$ and orientations of $\theta_e = \pm\pi/4, \pm 3\pi/4$. Considering only the part of Eq. (17) governing the dynamics of $y(t)$ and $\theta(t)$, the points $(y, \theta) = (y_e, \theta_e)$ are equilibrium points of this subsystem. [Formally, these points are called *relative equilibria* [38] of the full dynamical system in Eq. (17).] Linear stability analysis then shows that these equilibrium points are marginally stable and that the linearized dynamics about the equilibrium is associated with a pair of purely imaginary eigenvalues. Moreover, utilizing the geometric symmetries in this system, it can be shown that even when considering the fully nonlinear dynamics of this system under large perturbations about equilibrium, the solutions exhibit *periodic orbits* in the (y, θ) components. Physically, these solutions correspond to wavelike trajectories along the wall, oscillating about the line $y=y_e$ of steady parallel translation. Figures 3(b) and 3(c) show trajectories of the swimmer's center $z_0(t)$ under two different initial conditions. Note the remarkable similarity to Fig. 1(b) which describes the motion of the two-sphere swimmer near a wall [24].

Using the relation $dy/d\theta = \dot{y}/\dot{\theta}$, Eq. (17) results in a separable nonlinear differential equation in y and θ , which can be solved explicitly as

$$\theta(y) = \frac{1}{2} \arcsin \left[\sin(2\theta_0) \exp \left(\frac{3}{2} \ln \frac{y}{y_0} - \frac{1}{4} \ln \frac{y^2 - \epsilon^2}{y_0^2 - \epsilon^2} \right) \right],$$

where (θ_0, y_0) is a starting point on the trajectory. Figure 4 shows a phase portrait of trajectories in (θ, y) plane of a swimmer with $\epsilon=0.2$ under different initial conditions for the range $-90^\circ \leq \theta \leq 90^\circ$. The region $-90^\circ < \theta < 0$ corresponds to swimming to the right (positive x direction), while the region $0 < \theta < 90^\circ$ corresponds to swimming to the left (negative x direction). The line $\theta=0$ separating between these regions corresponds to purely vertical motion of the swimmer away from the wall. The lines $\theta=\pm 90^\circ$ correspond to vertical motion toward the wall. Since the phase portrait is 180° -periodic in the θ direction, Fig. 4 gives a complete characterization of the dynamical system (17) describing the behavior of the swimmer. The results are remarkably similar

to the predictions in [24] for the two-sphere swimmer (see the phase portrait in Fig. 2(b) of [24]).

V. CONCLUDING DISCUSSION

An important observation is that our procedure of matching inner and outer solutions is essentially an approximation since it assumes that the distance between the swimmer and the wall is large compared to the size of the swimmer. Obviously, this assumption does not always hold in our simulations. Note that this is also the case in the theoretical models in [24]. Nevertheless, the experimental results in [25] corroborate the predictions in [24], showing that this approximation is valid, at least qualitatively, even for small separations.

To summarize, the dynamics of a simple two-dimensional swimmer model interacting with a no-slip wall has been explicitly formulated and analyzed. The swimmer model captures a number of dynamical features proposed or directly observed by other works using independent approaches and suggests that the model is a useful one. Moreover, it also supports the idea that many qualitative phenomena involving low-Reynolds-number swimmers can be captured within two-dimensional models.

Some directions for future extension are as follows. First, a possible way to find more accurate (and complicated) solutions is to systematically apply asymptotic matching tech-

niques [39] and incorporate correction terms of higher order. However, in order to do so, it is necessary to make further physical assumptions on how the treadmilling swimmer responds to the presence of an ambient strain and shear. A second extension is replacing the no-slip wall with a *free surface*, which is exploited in the locomotion mechanism of some species of crawling water snails [40]. In the case of a flat surface, the solution is obtained by simply placing mirror-image singularities at the reflected point \bar{z}_0 . The case where the free surface is allowed to deform is currently investigated in [41] using complex variable techniques. Another possible generalization is to consider a boundary with partial slip condition [42] and analyze the influence of varying the slip length on the dynamic behavior. Finally, applying the techniques outlined here to account for more realistic models of swimmers and more complicated geometries is also a challenging open problem. As a preliminary step in this direction, analysis of swimming near a gap in the wall in two dimensions is currently under investigation [43].

ACKNOWLEDGMENTS

We thank the California Institute of Technology, where this work has been carried out. D.G.C. acknowledges useful discussions with Ophir Samson. Y.O. thanks Bikura program of the Israel Science Foundation for its support. We thank the anonymous referees for their useful comments and for bringing Ref. [23] to our attention.

-
- [1] E. Lauga and T. R. Powers, Rep. Prog. Phys. **72**, 096601 (2009).
 - [2] T. J. Pedley and J. O. Kessler, Annu. Rev. Fluid Mech. **24**, 313 (1992).
 - [3] R. Dreyfus, J. Baudry, M. L. Roper, M. Fermigier, H. A. Stone, and J. Bibette, Nature (London) **437**, 862 (2005).
 - [4] G. Kosa, M. Shoham, and M. Zaaroor, IEEE Trans. Rob. Autom. **23**, 137 (2007).
 - [5] E. M. Purcell, Am. J. Phys. **45**, 3 (1977).
 - [6] J. Happel and H. Brenner, *Low Reynolds Number Hydrodynamics* (Prentice-Hall, New Jersey, 1965).
 - [7] S. Kim and S. J. Karrila, *Microhydrodynamics* (Butterworth-Heinemann, Boston, 1991).
 - [8] A. Shapere and F. Wilczek, J. Fluid Mech. **198**, 557 (1989).
 - [9] A. Najafi and R. Golestanian, Phys. Rev. E **69**, 062901 (2004).
 - [10] J. E. Avron, O. Kenneth, and D. H. Oakmin, New J. Phys. **7**, 234 (2005).
 - [11] H. Brenner, J. Fluid Mech. **12**, 35 (1962).
 - [12] D. F. Katz, J. R. Blake, and S. L. Paverifontana, J. Fluid Mech. **72**, 529 (1975).
 - [13] D. F. Katz, J. Fluid Mech. **64**, 33 (1974).
 - [14] E. Lauga, W. R. DiLuzio, G. M. Whitesides, and H. A. Stone, Biophys. J. **90**, 400 (2006).
 - [15] J. Cosson, P. Huitorel, and C. Gagnon, Cell Motil. Cytoskeleton **54**, 56 (2003).
 - [16] A. P. Berke, L. Turner, H. C. Berg, and E. Lauga, Phys. Rev. Lett. **101**, 038102 (2008).
 - [17] T. Kaya and H. Koser, Phys. Rev. Lett. **103**, 138103 (2009).
 - [18] G. Zilman, J. Novak, and Y. Benayahu, Mar. Biol. (Berlin) **154**, 1 (2008).
 - [19] K. Drescher, K. C. Leptos, I. Tuval, T. Ishikawa, T. J. Pedley, and R. E. Goldstein, Phys. Rev. Lett. **102**, 168101 (2009).
 - [20] L. J. Fauci and A. McDonald, Bull. Math. Biol. **57**, 679 (1995).
 - [21] M. Ramia, D. L. Tullock, and N. Phan-Thien, Biophys. J. **65**, 755 (1993).
 - [22] J. P. Hernandez-Ortiz, C. G. Stoltz, and M. D. Graham, Phys. Rev. Lett. **95**, 204501 (2005).
 - [23] R. Zargar, A. Najafi, and M. F. Miri, Phys. Rev. E **80**, 026308 (2009).
 - [24] Y. Or and R. M. Murray, Phys. Rev. E **79**, 045302(R) (2009).
 - [25] S. Zhang, Y. Or, and R. M. Murray, Proc. IEEE American Control Conference (ACC), 2010 (to be published), preprint and movies are available online at www.technion.ac.il/~izi/research/low_Re_swim/acc2010
 - [26] K. Ehlers, A. Cherman, J. Koiller, J. Delgado, R. Montgomery, and F. Duda, Proc. 3rd Symposium on Hamilton Systems and Celestial Mechanics, 1998 (HAMSYS-98), edited by J. Delgado, E. A. Lacomba, E. Perez-Chavela, and J. Llibre (World Scientific Publishing, Singapore, 2000).
 - [27] A. M. Leshansky and O. Kenneth, Phys. Fluids **20**, 063104 (2008).
 - [28] L. E. Becker, S. A. Koehler, and H. A. Stone, J. Fluid Mech. **490**, 15 (2003).

- [29] M. J. Lighthill, *Commun. Pure Appl. Math.* **5**, 109 (1952).
- [30] T. Ishikawa, M. P. Simmonds, and T. J. Pedley, *J. Fluid Mech.* **568**, 119 (2006).
- [31] J. R. Blake, *Bull. Aust. Math. Soc.* **5**, 255 (1971).
- [32] W. E. Langlois, *Slow Viscous Flows* (Macmillan, New York, 1964).
- [33] C. Pozrikidis, *Boundary Integral and Singularity Methods for Linearized Viscous Flow* (Cambridge University Press, Cambridge, 1992).
- [34] J. R. Blake and A. T. Chwang, *J. Eng. Math.* **8**, 23 (1974).
- [35] G. K. Batchelor, *An Introduction to Fluid Dynamics* (Cambridge University Press, Cambridge, 1967).
- [36] J. R. Blake, *Math. Proc. Cambridge Philos. Soc.* **70**, 303 (1971).
- [37] A. M. Leshansky, O. K. O. Gat, and J. E. Avron, *New J. Phys.* **9**, 145 (2007).
- [38] J. E. Marsden, *Lectures on Mechanics* (Cambridge University Press, New York, 1992).
- [39] H. J. Hinch, *Perturbation Methods* (Cambridge University Press, Cambridge, 1991).
- [40] S. Lee J. W. M. Bush, A. E. Hosoi, and E. Lauga, *Phys. Fluids* **20**, 082106 (2008).
- [41] D. G. Crowdy, S. Lee, O. Samson, A. Hosoi, and E. Lauga (unpublished).
- [42] E. Lauga and H. A. Stone, *J. Fluid Mech.* **489**, 55 (2003).
- [43] D. G. Crowdy and O. Samson (unpublished).